ACS APPLIED NANO MATERIALS

December 2018
Volume 1
Number 12
pubs.acs.org/acsanm

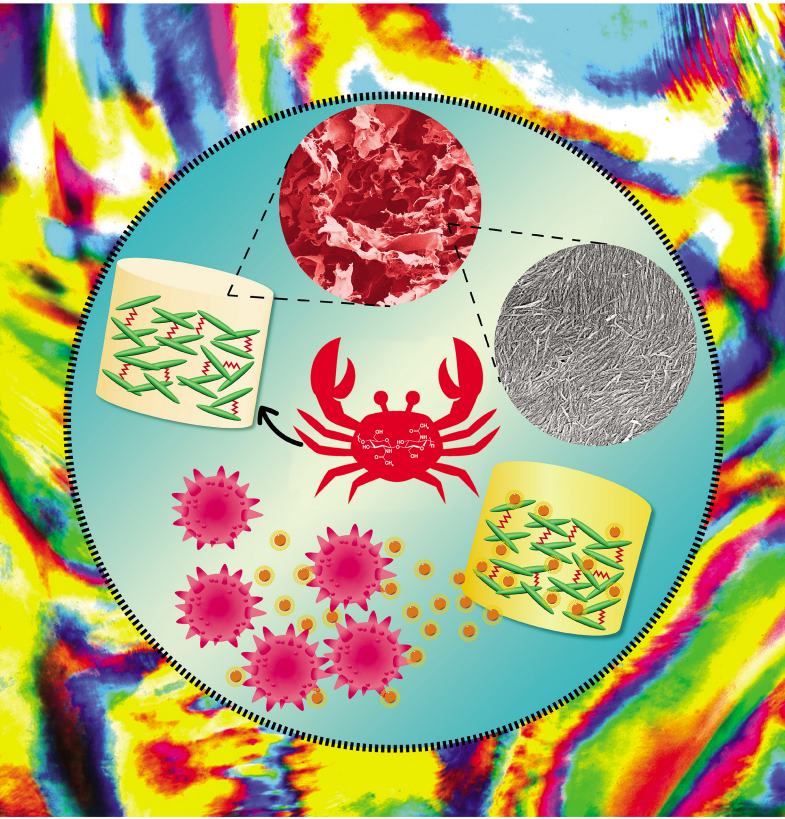

ACS Publications
Most Trusted. Most Cited. Most Read.

www.acs.org

ACS APPLIED NANO MATERIALS
Cite This: ACS Appl. Nano Mater. 2018, 1, 6790−6799
Article
www.acsanm.org

Chemically Cross-Linked Chitin Nanocrystal Scaffolds for Drug Delivery

Xianfeng Ou, Jingqi Zheng, Xiujuan Zhao, and Mingxian Liu*

Department of Materials Science and Engineering, Jinan University, Guangzhou 510632, China

Supporting Information

ABSTRACT: Chitin nanocrystals (ChNCs), prepared by acid hydrolysis of chitin, exhibit a uniform needlelike morphology and high dispersion stability in aqueous solutions, which makes them good candidates for drug delivery. Porous ChNC scaffolds were freeze-dried from different concentrations of ChNC dispersions and then cross-linked by a reaction with glutaraldehyde. Various techniques, including scanning electron microscopy, Fourier transform infrared spectroscopy, X-ray diffraction, thermogravimetric analysis, and testing of mechanical properties, porosity, and swelling properties, were used to characterize the structure of chemically cross-linked chitin nanocrystal (XChNC) scaffolds. The compressive mechanical strength, density, porosity, and water absorption rate of XChNC scaffolds were dependent on the concentration of ChNCs. XChNC scaffolds showed interconnected pores with a mean pore size of ∼65 μm diameter. Curcumin was used as a model drug and loaded into the XChNC scaffold by encapsulation in Tween 20 micelles. The drug release period from XChNC scaffolds was determined to be 540 min in phosphate-buffered saline (PBS) at pH 5.3 and 780 min in PBS at pH 7.4. Cytotoxicity experiments using human breast adenocarcinoma cells (MCF-7) revealed that released curcumin inhibited the proliferation of MCF-7 cells. All of the results show that XChNC scaffolds exhibit great potential for tissue-engineering and drug-delivery applications.

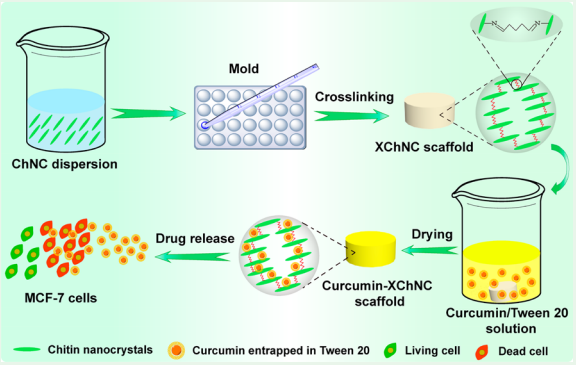

KEYWORDS: *chitin nanocrystals, scaffold, cross-linking, drug delivery, curcumin, cytotoxicity*

INTRODUCTION

Renewable and biodegradable biopolymers are popular in the fields of medical engineering and biotechnology. Several promising biopolymers from natural sources have been extracted and studied for tissue engineering and drug delivery, including collagen, cellulose, silk fibroin, chitin, starches, and natural rubbers. Among them, chitin is a readily available polysaccharide obtained from living organisms, such as crabs, shrimp, and insects, and chitin nanocrystals (ChNCs) are used to support their exoskeleton.[1−3] Chitin is composed of 2-acetamido-2-deoxy-D-glucose and consists of crystalline and amorphous domains, such as cellulose and starch.[4,5] ChNCs can be obtained by acid hydrolysis,[6] TEMPO-mediated oxidation,[7] and mechanical treatments[8] to degrade the amorphous domains of chitin. In comparison with bulk chitin, rodlike ChNCs with high aspect ratios and high longitudinal moduli[9] are employed as filling materials to enhance the mechanical properties of polymers.[10,11] ChNCs exhibit a uniform needlelike morphology with lengths and widths of 100−500 and 15−30 nm, respectively. The aspect ratio of ChNCs is 3−16. The high aspect ratio of ChNCs is a critical factor for self-organization into chiral nematic liquid-crystal phases. Needlelike ChNCs have a high modulus and strength along their long axes, ensuring their high reinforcing ability.[1] Needlelike ChNCs also have a high specific lateral surface area, endowing them with appropriate adsorption characteristics for drug molecules. Moreover, amino groups on needlelike ChNCs are prone to reacting with cross-linking agents, and a network structure between adjacent ChNC molecules tends to form. Because of their excellent properties of low density, abundant surface hydroxyl groups and good biocompatibility, ChNCs have been extensively studied as sensors, biorecognition elements, oil-in-water emulsions, and tissue scaffolds. For example, ChNCs have been used as a reinforcing material for rubber to enhance the tensile strength of conductive composites.[12] ChNCs functionalized by a fluorescent imidazoisoquinolinone dye have been shown to result in selective interactions with their corresponding binding proteins.[13] Oil-in-water emulsions have been stabilized by ChNCs because they have an interdroplet network structure.[14] ChNCs have also been combined with poly(3-hydroxybutyrate-*co*-3-hydroxyvalerate) to form porous composites with macro- and micropores, which were used as tissue-engineering scaffolds for enhancing the adhesion of human adipose-derived stem cells.[15] However, to the best of our knowledge, no research has

Received: September 10, 2018
Accepted: November 9, 2018
Published: November 9, 2018

DOI: 10.1021/acsanm.8b01585
ACS Appl. Nano Mater. 2018, 1, 6790−6799

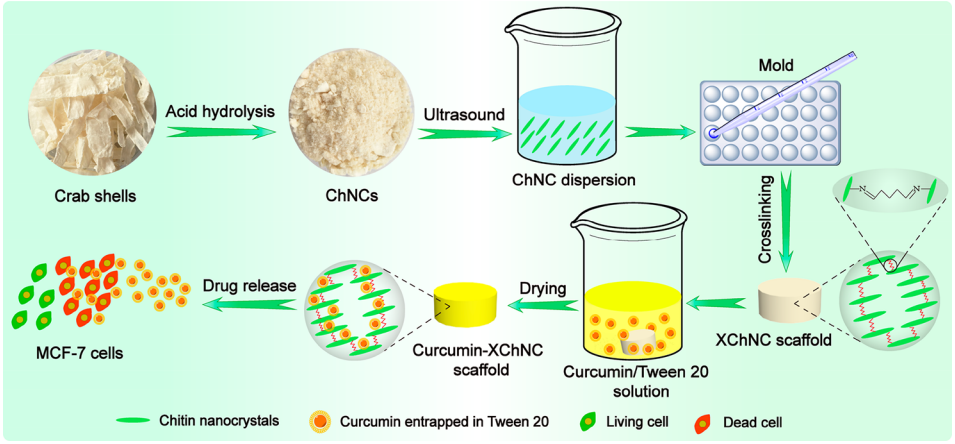

Figure 1. Schematic illustration of the synthesis of the XChNC scaffold and the process of drug release from the curcumin-XChNC scaffold.

been published on the development of ChNCs for drug-delivery applications.[16,17]

ChNCs and cellulose nanocrystals are similar in chemical structure and morphology, while the only difference is the side group on site C2. The C2 of cellulose nanocrystals is connected to a hydroxyl group (−OH), while the C2 of ChNCs is connected to an acetamido group ($-NHCOCH_3$). To date, many studies have been conducted in the field of cellulose nanocrystals for drug-delivery carrier applications.[18−21] Cellulose nanocrystal films loaded with curcumin have been used as an antimicrobial drug-delivery system in a diabetic wound dressing, and the drug was steadily released from the film for 36 h with a total release of 98.9%.[22] Cellulose nanocrystals have also been incorporated into chitosan nanoparticles as a carrier system for the controlled release of repaglinide.[23] As alternative polysaccharide nanocrystals, ChNCs also have high surface areas, biocompatibility, anticoagulant properties, and antibacterial properties. Therefore, ChNCs are promising nanomaterials for drug delivery both in vitro and in vivo.

Porous polymer scaffolds are commonly used to improve the drug-loading capacity because of their high porosity. Generally, porous nanocrystal scaffolds have been prepared by freeze-drying, solvent extraction, freeze extraction, freeze gelation, powder compaction, and phase inversion.[24] Porous nanocrystal scaffolds not only have ultralow densities and high strength properties but also have interconnected pore structures and a high degree of porosity for loading bioactive drug molecules.[25] For instance, it has been reported that a basic fibroblast growth factor and curcumin entrapped in gelatin microspheres were loaded into porous collagen/cellulose nanocrystal scaffolds, and the drug was sustainably released from scaffolds for skin tissue engineering and burn infection treatment.[26,27] Chitosan and gelatin composite sponges also had suitable pore structures, and the percent release of curcumin loaded into these sponges reached a maximum of 91% in 96 h.[28] Attributed to a regular pore size and fibrillar structure, a chitosan/sodium alginate sponge as a drug carrier has been loaded with curcumin and showed long-term drug release for 20 days.[29] ChNCs can be nanocomponents for reinforcing polymer scaffolds for different biomedical applications. For example, electrospun chitosan-based nanocomposite mats have been reinforced with ChNCs for wound dressings.[30] Previously, we also prepared chitosan/ChNC composite scaffolds by solution mixing and freeze-drying for tissue-engineering applications.[9] However, it is a challenge to prepare porous scaffolds using ChCNs by themselves.

In this study, rodlike ChNCs were prepared by acid hydrolysis, and the morphology, liquid-crystalline behavior, and rheological properties of the ChNC dispersion were studied. Porous ChNC scaffolds prepared by freeze-drying were further cross-linked by glutaraldehyde to improve their stability in aqueous solution. Subsequently, curcumin encapsulated in Tween 20 was loaded into cross-linked ChNC (XChNC) scaffolds. A series of characterizations of the scaffolds were conducted to evaluate the chemical composition, crystal structure, and mechanical and thermal behavior. Furthermore, the release behavior of curcumin from porous XChNC scaffolds was studied in vitro. Curcumin showed a noticeable effect of inhibiting the growth of human breast adenocarcinoma cells (MCF-7). Therefore, porous XChNC scaffolds could become promising materials for drug-delivery, tissue-engineering, and wound-dressing applications.

MATERIALS AND METHODS

Materials. Crab shells were supplied by Wuhan Hezhong Biochemical Manufacturing Co., Ltd., China. Curcumin powder (purity of ∼95%) was obtained from Nanogong Sanxin Natural Pigment Ltd., China. Acridine orange/ethidium bromide (AO/EB) staining reagent was purchased from Beijing Solarbio Science & Technology Co., Ltd., China. CCK-8 reagent was supplied from BestBio Biology Co., Ltd., China. Water was filtered by a Milli-Q water system (resistivity >18.2 MΩ/cm). Other chemicals of analytical grade were purchased from Aladdin Industrial Corp.

Preparation of the ChNC Powder and ChNC Dispersion. The ChNC powder was prepared by acid hydrolysis according to a previous study.[31] Briefly, 20 g of crab shells and 3 mol/L HCl were added to a three-necked flask with oil bath heating at 104 °C for 3 h. After acid hydrolysis, the mixture was washed by centrifugation with ultrapure water at 4000 rpm for 10 min. This process was repeated three times to remove excess acid and the amorphous phase. The suspension was then dialyzed in running water until the pH value of the suspension was near 7.0. Finally, the ChNC powder was collected by a SCIENTZ-12ND vacuum freeze-dryer (Ningbo Scientz Biotechnology Co., Ltd., China). The ChNC powder was then added to ultrapure water to obtain the ChNC concentrations of 2, 3, 5, 10, and 15 wt %. To prepare a homogeneous dispersion with uniformly distributed nanocrystals, the ChNC dispersion was treated by an ultrasonic cell disruptor (JY99-IIDN, Ningbo Scientz Biotechnology Co., Ltd., China).

Fabrication of XChNC Scaffolds. Different concentrations of the ChNC dispersion obtained from the previous step were poured into a 24-well plate. Different amounts of ChNC scaffolds were obtained

DOI: 10.1021/acsanm.8b01585
ACS Appl. Nano Mater. 2018, 1, 6790−6799

after freeze-drying. To prepare XChNC scaffolds, ChNC scaffolds were immersed in 2.5 vol % glutaraldehyde for 12 h at room temperature, subsequently washed with absolute ethanol and ultrapure water, and then freeze-dried.[32,33]

Preparation of Curcumin-Loaded XChNC (Curcumin-XChNC) Scaffolds. Using a high-speed blender, a curcumin aqueous solution with a concentration of 1.0 mg/mL was prepared with Tween 20 as an emulsifier.[34] Dry XChNC scaffolds were soaked in a curcumin/Tween 20 solution in the dark for 24 h. The curcumin-loaded scaffolds were gently blotted with filter paper before drying them at 40 °C. Curcumin has strong interactions with ChNCs, so the adsorption of curcumin on the surfaces of the scaffold was considered uniform with the soaking method. Washing the drug-loaded scaffold with ethanol may lead to some of the curcumin being lost. This would yield inaccurate data for drug-release studies. The synthesis of the XChNC scaffold and the process of drug release from the curcumin-XChNC scaffold are schematically illustrated in Figure 1.

Characterization of the ChNC Dispersion. The morphology of ChNCs was analyzed by transmission electron microscopy (TEM; JEM-2100F, JEOL Ltd., Japan), scanning electron microscopy (SEM; Ultra 55, Zeiss, Germany), and atomic force microscopy (AFM; Bioscope Catalyst Nanoscope-V, Bruker Instruments Ltd., USA). The particle size distribution and ζ potential of the ChNC dispersion were obtained using a Nano ZS ζ-potential analyzer (Malvern Instruments Co., U.K.). The samples for TEM, SEM, AFM, particle size distribution, and ζ-potential testing were prepared with a dilute ChNC solution of 0.05 wt %. Images of the ChNC dispersion were observed with a polarized optical microscope (BX51, Olympus, Japan). The rheological behavior of the ChNC dispersion was measured by a hybrid rheometer (TA Discovery HR-2, USA) using parallel plates with a diameter of 40 mm at 30 °C. The shear rate of the dynamic viscosity was measured from 10^{-3} to 10^{3} s^{-1}, while the dynamic frequency sweep of the storage modulus (G') and loss modulus (G'') were analyzed from 10^{-1} to 10^{2} rad/s.

Characterization of the Scaffolds. *Stability Evaluation.* To compare the stability of the ChNC and XChNC scaffolds, the scaffolds (5 mm in height and 10 mm in diameter) were immersed in a 10% serum solution and a phosphate-buffered saline (PBS) solution (pH 7.4) and observed for 14 days.

Mechanical Property Tests. A compressive performance of the XChNC scaffolds was conducted using a mechanical testing instrument (UTM-Q422, China) at room temperature with a speed of 2 mm/min. Before the compression of scaffolds in a wet state was tested, the samples were immersed in a PBS solution (pH 7.4) at room temperature for 24 h. According to Hooke's law, in the stage of material elastic deformation, stress is positively correlated to strain, and the correlation coefficient is referred to as the elastic modulus. The elastic modulus of each sample was obtained by fitting a line with software. All results were reliably obtained by testing five replicate samples.

Density, Porosity, and Water Absorption Measurements. Cylinder-shaped XChNC scaffolds were used to determine the density, porosity, and water absorption. The density of the XChNC scaffolds was calculated using the formula

$$\text{density} = \frac{m}{\pi(d/2)^2 h} \times 100\%$$

where m, d, and h are the weight, diameter, and height of the samples, respectively.

The porosity test of the scaffolds was analyzed by a liquid displacement method with absolute ethanol according to a previous study.[9] Different amounts of XChNC scaffolds were soaked in absolute ethanol at room temperature for 24 h. Excess ethanol was removed from the sample surfaces before being measured. The porosity of the XChNC scaffolds was determined by the formula

$$\text{porosity} = \frac{m_2 - m_1}{\rho V_1} \times 100\%$$

where m_2, m_1, ρ, and V_1 are the weight of the samples after and before immersion in absolute ethanol, the density of absolute ethanol, and the volume of the samples before immersion, respectively.

To determine the water absorption of the scaffolds, the samples were prepared via immersion in ultrapure water for 24 h. Excess water was removed from the sample surfaces before being measured. The water absorption rate of the scaffolds was determined by the equation

$$\text{water absorption} = \frac{m_2 - m_1}{m_1} \times 100\%$$

where m_2 and m_1 are the weight of the sample after and before immersion in ultrapure water, respectively. Both the mean and standard deviation were reliably obtained by testing five parallel samples.

SEM. The porous morphology of the XChNC scaffolds was analyzed by SEM (Ultra 55, Zeiss, Germany) at a voltage of 5 kV. The samples were prepared by coating a thin layer of gold on the samples prior to characterization.

Fourier Transform Infrared (FTIR) Spectroscopy. The FTIR spectra of ChNCs, XChNCs, curcumin, and curcumin-XChNCs were acquired on a Thermo FTIR instrument (Nicolet iS50, Thermo Fisher Scientific Ltd., USA) with a KBr tablet. The scanned wavenumber range was from 4000 to 500 cm^{-1}.

X-ray Diffraction (XRD). The XRD patterns of ChNCs, XChNCs, curcumin, and curcumin-XChNCs were characterized by an X-ray diffractometer (MiniFlex-600, Rigaku Corp., Japan). The scanning angle was from 5° to 50° with a scanning speed of 10°/min.

Thermogravimetric Analysis (TGA). To study the thermal stability and composition of the materials, 5 mg each of ChNCs, XChNCs, curcumin, and curcumin-XChNCs were tested with a TGA instrument (Mettler Toledo, Switzerland). The range of the heating temperature was from 50 to 500 °C with a heating rate of 10 °C/min under a nitrogen atmosphere.

Loading Efficiency and Entrapment Efficiency. Dried XChNC scaffolds were placed in a 10 mg/mL curcumin/Tween 20 solution in the dark for 24 h. The concentration of the curcumin solution was determined using an ultraviolet spectrophotometer (UV-2550, Shimadzu Instrument Ltd., China) at 425 nm. The drug-loading efficiency and entrapment efficiency of the XChNC scaffolds were quantified using the following equations:

$$\text{loading efficiency} = \frac{\text{amount of loaded curcumin}}{\text{weight of curcumin loaded XChNC scaffold}} \times 100\%$$

$$\text{entrapment efficiency} = \frac{\text{total amount of curcumin} - \text{free curcumin}}{\text{total amount of curcumin}} \times 100\%$$

In Vitro Drug-Release Study. Curcumin-XChNC scaffolds were immersed in 25 mL of PBS (pH 7.4 and 5.3) and incubated in a shaker (HS-100B, Shanghai Hanqiang Instrument Co., Ltd., China) at 37 °C with a speed of 60 rpm. After a certain time of release, 0.5 mL of the release solution was taken from the release medium, and 0.5 mL of fresh PBS was returned to the release medium. The released drug was quantified by an ultraviolet spectrophotometer at a wavelength of 425 nm. The drug-release behavior was evaluated by the relative curcumin release ratio according to the equation[35]

$$\text{relative release ratio} = \frac{C_t}{C_\infty} \times 100\%$$

where C_t is the concentration of the released curcumin at time t and C_∞ represents the concentration of the released curcumin at 18 h.

Cytotoxicity. First, 1-mm-thick slices of scaffolds were sterilized by γ irradiation with an irradiation dose of 2.5 kGy. MCF-7 cells were cultured in Dulbecco's modified Eagle's medium (DMEM; Gibco/Thermo Fisher Scientific Ltd., USA) in a humidified atmosphere with 5% CO_2 at 37 °C. Then, MCF-7 cells were seeded on the scaffolds in 96-well plates (5×10^3 cells/well). After the MCF-7 cells were

DOI: 10.1021/acsanm.8b01585
ACS Appl. Nano Mater. 2018, 1, 6790−6799

incubated with scaffolds for 24 and 72 h, an AO/EB staining assay was used to observe dead and living cells using a fluorescence microscope (XDY-2, Guangzhou Liss Optical Instrument Co., Ltd., China). Similarly, CCK-8 assay was performed after cells were cultured for 1, 3, and 5 days. Cells were washed with fresh PBS. Then, fresh DMEM and CCK-8 reagent (volume ratio = 10:1) were added to the wells of the 96-well plates. The absorbance was measured using a microplate reader at a wavelength of 450 nm. The cell viability was calculated as the absorbance ratio of the sample to the control group.

RESULTS AND DISCUSSION

Characterization of the ChNCs. ChNCs were successfully prepared from crab shells by acid hydrolysis. ChNC concentrations of 2−15 wt % aqueous solution were dispersed homogeneously by ultrasound, as shown in Figure 2a. Because of their high viscosity, 10 and 15 wt % ChNCs in bottles maintained their shape when inverted, while the dispersion with a concentration below 5 wt % was fluid. Therefore, ChNC dispersions with concentrations greater than 10 wt % are injectable by a syringe with a needle diameter of 0.6 mm (Figure 2b). The ChNC dispersion with a concentration of 0.05 wt % was used for morphology analysis and particle size distribution determination. The morphology of ChNCs was then characterized by TEM, SEM, and AFM (Figure 2c−e). ChNCs exhibited a uniform needlelike morphology, showing a wide length and a width distribution of 100−500 and 15−30 nm, respectively. Therefore, ChNCs had an aspect ratio of 3−16. These results are consistent with a previous study.[31] Figure 2f shows the size distribution of the ChNC dispersion after sonication. The distribution of the particle size ranged from 51 to 295 nm with a mean size of 106 nm, and the ζ potential of the ChNC dispersion was +44.7 mV. The size distribution of ChNCs was smaller than that measured by morphology observation because the laser particle size analyzer is based on the theory of a uniform sphere. The ChNC dispersion had good stability and colloidal behavior because of the positive charge of the protonated amino groups, verifying the ζ-potential result.[36] ChNCs exhibited a needlelike nanostructure and were uniformly dispersed in aqueous solution, which is beneficial for forming porous scaffolds by freeze-drying the ChNC dispersion and is also a critical factor for improving the mechanical properties of the scaffolds. A previous study showed that ChNCs with a high longitudinal modulus (150 GPa) can be used as effective reinforcement materials for alginate hydrogels.[37]

The behavior of rodlike ChNCs with good stability in aqueous solution was further illustrated by polarized optical microscopy (Figure 3). When the ChNC concentration was 3 wt % or less, no birefringence phenomenon was observed because the ChNCs are in the isotropic phase. A small amount of crystalline liquid surrounded by the isotropic phase was observed in 5 wt % ChNCs; therefore, isotropic and liquid-crystalline phases coexisted at this concentration. The liquid-crystalline phase increased with increasing ChNC content. The birefringence phenomenon and fingerprint texture were clearly observed at a concentration of 10 wt %. The liquid-crystalline phase was completely formed when the ChNC concentration was greater than 10 wt %, which is attributed to a self-assembling process of parallel alignments of the anisotropic crystallites (chiral nematic order).[38−40] The results from polarized optical microscopy explain why rodlike ChNCs had good stability in aqueous solution, and the dispersion was injectable at high concentrations.

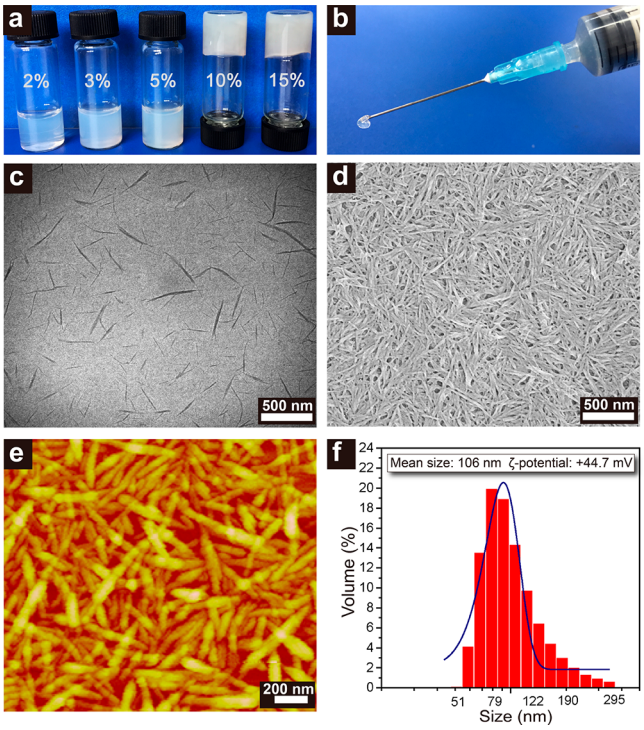

Figure 2. Appearance of different concentrations of ChNC aqueous dispersions (a). Injectable hydrogel consisting of 15 wt % ChNCs (b). TEM (c), SEM (d), AFM height phase (e), and particle size distribution (f) of ChNCs.

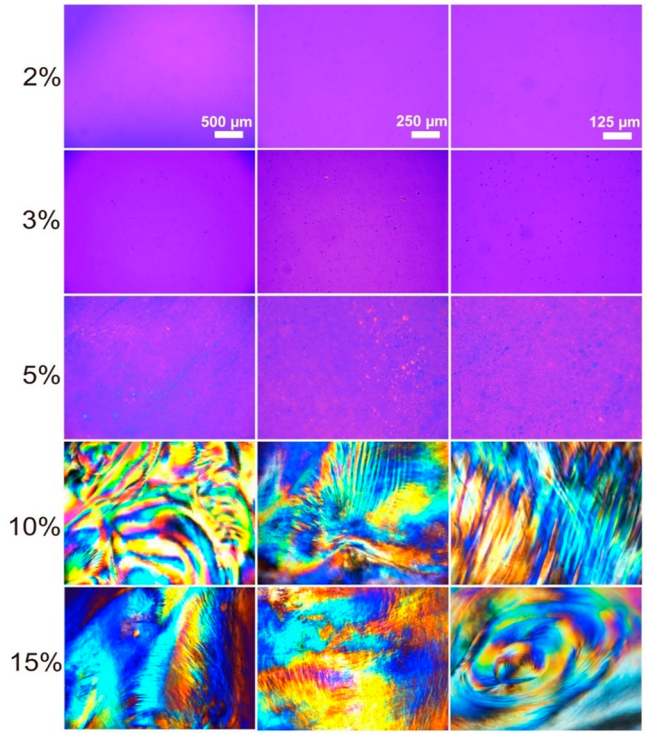

Figure 3. Polarized optical microscopy images of different concentrations of ChNC dispersions with different magnifications of 50×, 100×, and 200×.

DOI: 10.1021/acsanm.8b01585
ACS Appl. Nano Mater. 2018, 1, 6790−6799

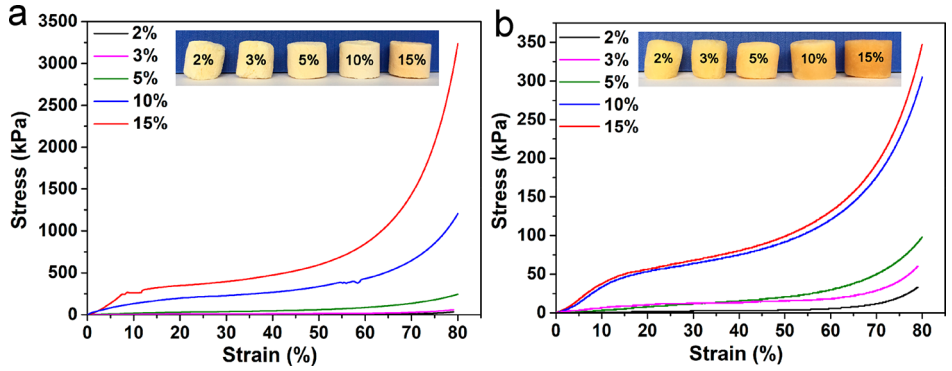

Figure 4. Compressive stress−strain curves of the XChNC scaffolds in a dry state (a) and in a wet state (b).

The sol−gel transition of ChNC dispersions was characterized by rheology testing. The storage modulus (G') and loss modulus (G'') versus frequency curves are shown in Figure S1a,b. The sol−gel transition of ChNC dispersions occurred above a critical concentration, and the intersection of the G' and G'' curves was the gel point. Above the intersection point, the state of a ChNC dispersion transformed from a liquid-like state to a solid-like state.[41] Both G' and G'' improved with increasing frequency and sample concentration. This suggests that a network structure was formed by fiber-like nanoparticles, especially at high concentrations. In a comparison of the curves of G' and G'', G' values for all concentrations of ChNCs were greater than the corresponding G'' values. Furthermore, G' and G'' of 15 wt % ChNCs were nearly not dependent on the angular frequency, suggesting the formation of a strong gel. G' and G'' with ChNC concentrations of 10 wt % or less overlapped at a low angular frequency and gradually separated with increasing angular frequency. This indicates that the rheological characteristics were frequency-dependent for these dispersions. The curve of the shear viscosity versus shear rate of ChNC dispersions is shown in Figure S1c. The viscosity slightly increased with increasing concentration of ChNCs, suggesting strong molecular interactions between the chitin chains. Moreover, the viscosity of different concentrations of ChNC dispersions decreased with increasing shear rate, indicating a typical shear-thinning behavior.[42] A previous study suggested that ChNCs are highly oriented in the shear direction, resulting in a weakening of the hydrogen-bonding interactions in the ChNC network.[43]

Stability Evaluation and Mechanical Properties of Porous XChNC Scaffolds. It is important to study the stability of ChNC scaffolds as drug-delivery carriers in physiological fluids. As shown in Figure S2a, 2, 5, and 15 wt % ChNC scaffolds absorbed water and swelled after immersion in serum on day 14 compared to day 1. Moreover, the structure of the 2 wt % ChNC scaffold was observed to be loose and the surface collapsed, while some white pieces of the 5 and 15 wt % ChNC scaffolds dispersed in water without shape collapse. Therefore, ChNC scaffolds without cross-linking are not stable and tend to break up in water. This is due to a large number of hydrophilic groups (hydroxyl, *N*-acetyl, and a small number of amino groups) on the ChNC surface, which hinders practical applications in loading and releasing drugs in physiological fluids. Additionally, the broken pieces affected the measurement of the drug concentration by spectrophotometry. The amino groups on the surface of the ChNCs were protonated in aqueous solution when the ChNC scaffold was soaked in water. Electrostatic repulsion between ChNC molecules was caused by protonated amino groups ($-NH_3^+$),[44] which forced the ChNC molecules in scaffolds to disperse in water. Moreover, hydrophilic groups (hydroxyl, *N*-acetyl, and amino groups) of ChNCs also made them easier to disperse in water. Thus, problems with untreated ChNC scaffolds immersed in water occurred, such as surface collapse, crack formation, and shape deformation. To increase the stability of the ChNC scaffolds, XChNC scaffolds were prepared by cross-linking the amino groups of ChNCs with a glutaraldehyde solution. XChNC scaffolds (2, 5, and 15 wt %) were tested similarly to ChNC scaffolds. In a comparison of day 14 to day 1, cross-linked scaffolds swelled slightly and maintained a 3D structure without dissolution or disintegration in serum. The reduction in the number of hydrophilic groups on the ChNCs weakened their interactions with water molecules.[32] As shown in Figure S2b, the result of the stability evaluation in PBS for 14 days was similar to that in serum. Thus, the XChNC scaffold exhibited improved stability in serum and PBS compared with the raw ChNC scaffold. This suggests that the XChNC scaffold has potential applications in vivo as a drug-delivery carrier.

As discussed above, XChNC scaffolds enable the stability in serum and a PBS solution to be maintained for a period of time. To further study the mechanical properties of XChNC scaffolds, compressive stress−strain curves of XChNC scaffolds in dry and wet states were investigated (Figure 4). The mechanical properties of the XChNC scaffolds are shown in Table S1. The inset pictures show the appearance of XChNC scaffolds in the dry and wet states. Because of the formation of a chromophoric imine group (−N═C−) by the cross-linking treatment, XChNC scaffolds showed a light-yellow-brown color in the dry state, and the color became slightly darker in the wet state. Either in the dry state or in the wet state, improved stiffness was observed with an increase of the concentration of ChNCs through tactile compression by fingers. As shown in the compressive stress−strain curves in the dry and wet states, the stress nearly linearly increased with increasing strain during the initial stage because of elastic deformation of the material. The stress in most curves exponentially increased with increasing compressive strain from 50% to 80%. Moreover, the compressive strength of XChNC scaffolds in both the dry and wet states dramatically increased with increasing concentrations of ChNCs. It can be concluded that the mechanical properties for all scaffold concentrations were clearly smaller in the wet state than in the dry state. For instance, the compressive strength of the XChNC scaffold with a 15 wt % ChNC concentration was 3237.58 kPa, while it was only 70.47 kPa for the 2 wt % sample

DOI: 10.1021/acsanm.8b01585
ACS Appl. Nano Mater. 2018, 1, 6790−6799

in the dry state. In contrast, the compressive strength of the XChNC scaffold was 33.17 and 347.83 kPa for 2 and 15 wt % concentrations in the wet state, respectively. The maximum load in the dry state of the XChNC scaffold with a 15 wt % concentration was 430.25 N, which was 9.29-fold greater than the result of 46.29 N in the wet state. Glutaraldehyde mainly reacts with the amino groups of chitin, which results in the formation of chromophoric imine groups (−N═C−) among ChNC molecules. As a result, ChNCs gradually form a stiff network structure via cross-linking, thus increasing the mechanical strength of the scaffolds.[45] Briefly, the improved mechanical integrity is satisfactory for applications in drug delivery in the dry and wet states.

Morphology, Porosity, and Water Absorption Ratio of XChNC Scaffolds. The morphology of the freeze-dried XChNC scaffolds was observed with SEM (Figure 5). The

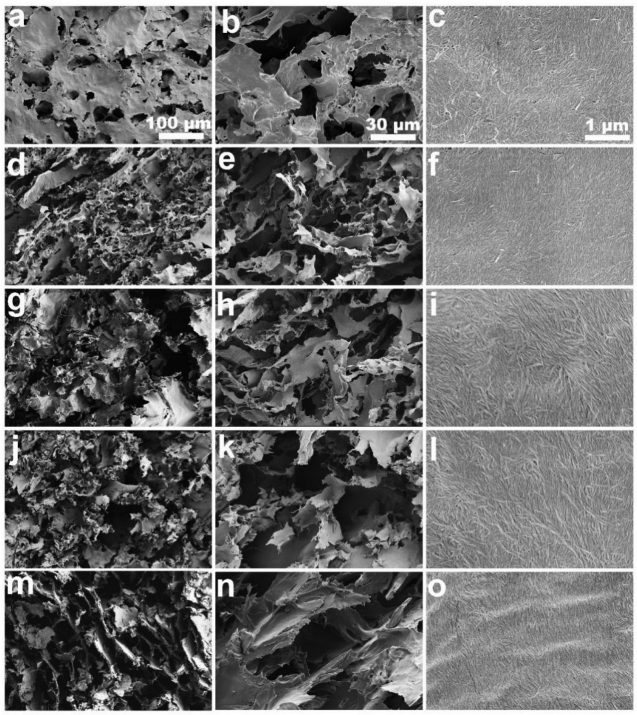

Figure 5. SEM images of freeze-dried XChNC scaffolds with different magnifications: 2 wt % XChNCs (a−c); 3 wt % XChNCs (d−f); 5 wt % XChNCs (g−i); 10 wt % XChNCs (j−l); 15 wt % XChNCs (m−o).

network structure of the XChNC scaffolds was composed of interconnected pores with diameters of 30−100 μm, and the formation of pores is attributed to the sublimation of ice crystals during freeze-drying.[46] With an increase in the concentration of ChNCs, the mechanical properties of the scaffolds became stiff and rigid. For instance, the pore wall of the 2 wt % XChNC scaffold was smooth and thin, while the pore wall of the 15 wt % scaffold was much thicker and stiffer. As shown in Figure 5m, XChNC scaffolds formed uniformly stratified pore structures at high nanocrystal concentrations. Moreover, through observation of the SEM images at higher magnifications (Figure 5c,f,i,l,o), it can be clearly seen that countless needlelike ChNCs are interrelatedly overlapped and uniformly distributed in the pore wall. Therefore, the freeze-dried XChNC scaffolds exhibited interconnected pores with high porosity, which is also described in the following analysis. The pore structure of scaffolds with a high surface area is beneficial for improving the drug-loading capacity.

The structural characteristics of the XChNC scaffolds are listed in Figure 6. With an increase in the concentration of ChNCs, the density of the XChNC scaffolds increased linearly from 0.026 to 0.16 g/cm^3 (Figure 6a). The ultralight weight of the XChNC scaffolds was also demonstrated in a previous study, where a scaffold was placed on a slender leaf tip without crushing it.[47] As previously stated, the density of the scaffold also affects the mechanical properties. The compressive strength of the scaffold increased with increasing scaffold density. The porosity of the XChNC scaffolds was in the range of 88.6−99.0% (Figure 6b), and the porosity slightly decreased with increasing ChNC concentration due to the formation of a more densely packed structure. The water uptake ratio of the 2 wt % scaffolds was 2377.7%, while it was 578.7% in the 15 wt % scaffold (Figure 6c). Two factors affect the water absorption ability of the scaffold. One factor is the hydrophilicity of the polymers, and the other is the porosity. Because there is only one component in the ChNC scaffold, the scaffold porosity mainly affects the water absorption. The decreased porosity leads to a decreased water absorption ratio because the spacing for water entry decreases at high ChNC concentrations. Therefore, the tunable porosity and water absorption ability of the XChNC scaffolds can meet practical requirements for drug delivery.

Chemical Structures of XChNC and Curcumin-XChNC Scaffolds. To investigate the chemical structures of XChNC and curcumin-XChNC scaffolds, the scaffold samples were measured by FTIR, XRD, and TGA (Figure 7). The FTIR spectra of ChNCs, XChNCs, curcumin, and curcumin-XChNCs are shown in Figure 7a. Characteristic peaks of the ChNCs were observed at 3463 cm^{-1} (O−H stretching), 3261 cm^{-1} (N−H stretching), 1661 and 1625 cm^{-1} (amide I), and 1559 cm^{-1} (amide II), which is consistent with the previous work.[48] In particular, the strong absorption bands at 1661 and 1625 cm^{-1} (amide I) suggest an α-chitin structure prepared from crab shells.[44] There was no significant difference between the FTIR spectra of ChNCs and XChNCs, likely because the new bonds of the imine bond (N═C) at 1655 cm^{-1} and the ethylenic bond (C═C)[49] at 1562 cm^{-1} after cross-linking overlapped with the absorption bands of amide I and amide II.[32] In a comparison of the spectra of XChNCs and curcumin-XChNCs, XChNCs incorporated with curcumin resulted in an increase in the band intensity at 3447 cm^{-1} (O−H stretching of XChNCs and curcumin) and 1074 cm^{-1}(C−O−C stretching vibrations of curcumin).[50] The results indicate that there were hydrogen-bonding interactions between curcumin and XChNCs. As shown in the XRD patterns in Figure 7b, the diffraction peaks of ChNCs appeared at 9.4° (020 plane), 19.3° (110 plane), 20.8° (120 plane), and 23.4° (130 plane), indicating the crystal structure of α-chitin.[48] The position and intensity of the XChNC diffraction peaks were similar to those in the ChNC pattern, suggesting that ChNCs retained their original crystalline structure after cross-linking with glutaraldehyde. The main diffraction peaks of curcumin appeared at 2θ = 17−28°, and an increase in the diffraction intensity of curcumin-XChNCs was observed at 23.4° as a result. Parts c and d of Figure 7 show thermal degradation of ChNCs, XChNCs, curcumin, and curcumin-XChNCs. ChNCs and XChNCs began to lose weight at 60 °C because of moisture loss. The initial degradation temperatures of ChNCs, XChNCs, curcumin, and curcumin-XChNCs were 234, 241,

DOI: 10.1021/acsanm.8b01585
ACS Appl. Nano Mater. 2018, 1, 6790−6799

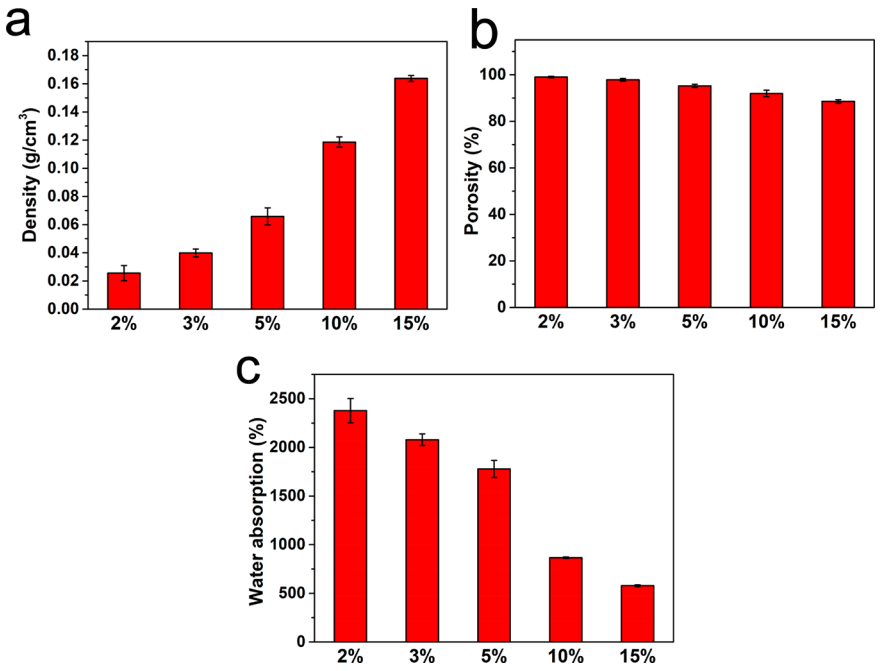

Figure 6. Density (a), porosity (b), and water absorption (c) of XChNC scaffolds.

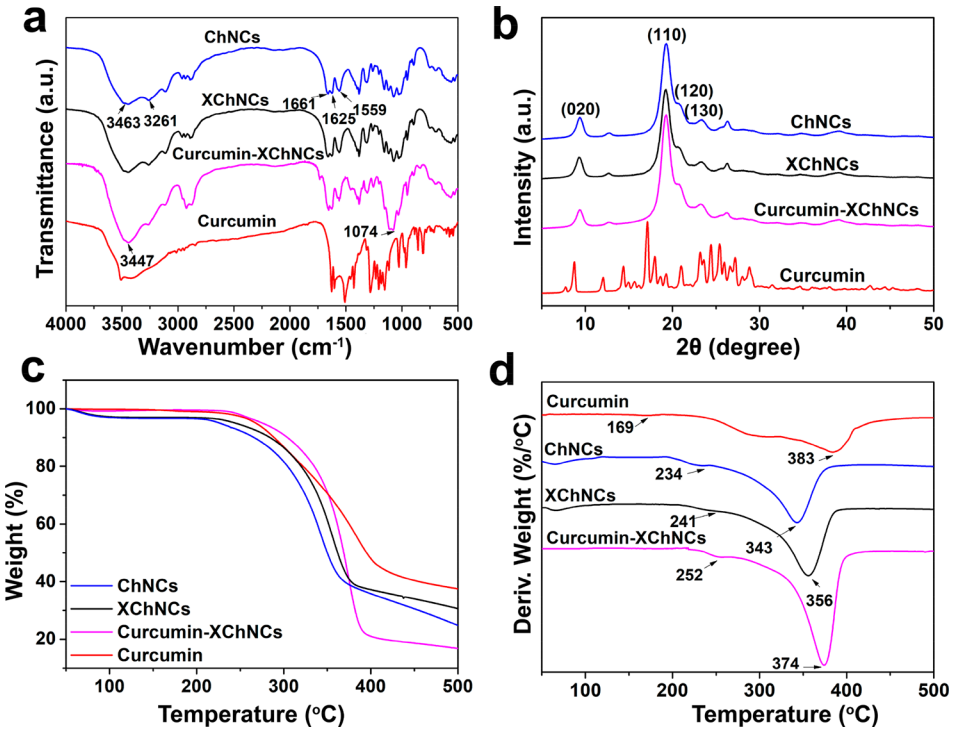

Figure 7. FTIR (a), XRD (b), TGA (c), and differential thermogravimetry (d) patterns for ChNCs, XChNCs, curcumin, and curcumin-XChNCs.

169, and 252 °C, respectively, and the maximum decomposition temperatures were 343, 356, 383, and 374 °C, respectively. The degradation temperatures of XChNCs increased by nearly 10 °C in comparison with those of ChNCs because of heat absorption due to decomposition of the N═C bond. Curcumin-XChNCs demonstrated an improved thermal stability compared to XChNCs as a result of the presence of curcumin.[51]

Drug-Loading and In Vitro Drug-Release Studies. The curcumin loading and release rate of XChNC scaffolds are crucial for applications as drug-delivery carriers. Curcumin with low water solubility was effectively loaded into scaffolds and released from scaffolds in an aqueous medium because curcumin was completely encapsulated in Tween 20 surfactant micelles. Curcumin-XChNC scaffolds exhibited a uniform yellow appearance (inset photograph in Figure 8a), suggesting that curcumin was homogeneously loaded in the scaffolds. The loading and entrapment efficiency of curcumin in XChNC scaffolds were calculated as 0.36% and 7.35%, respectively. Figure 8b shows the drug-release curves of curcumin-XChNCs

DOI: 10.1021/acsanm.8b01585
ACS Appl. Nano Mater. 2018, 1, 6790−6799

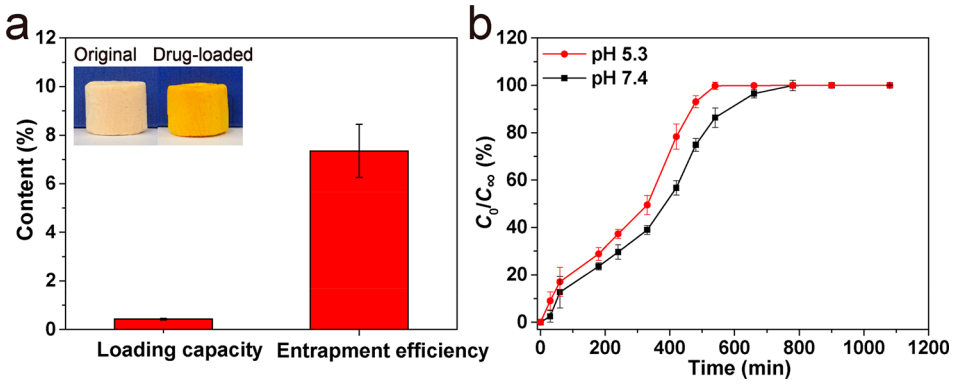

Figure 8. Drug-loading capacity and entrapment efficiency of XChNC scaffolds (the inset photograph shows the appearance of the original and drug-loaded XChNC scaffolds) (a) and drug-release curves of curcumin-XChNC scaffolds in PBS at pH 7.4 and 5.3 (b).

in a PBS solution at pH 7.4 and 5.3. The scaffolds exhibited a burst release in the first 60 min, and the release ratios reached 12 and 17% at pH 7.4 and 5.3, respectively. A burst release of curcumin is beneficial in the treatment of wounds because the drug can be released swiftly upon reaching the lesion area. Then, as the release time increased, the drug release slightly increased in PBS at the two different pH values. After 300 min, the drug release ratio from the scaffold was 35% at pH 7.4, and it was 45% at pH 5.3. At 500 min, 78% of curcumin was released from the scaffold at pH 7.4, while 95% of curcumin was released at pH 5.3. After 500 min, the drug release became slower, and the release was observed to cease at 540 min (pH 5.3) and 780 min (pH 7.4). Briefly, the drug-release rate at pH 5.3 was much faster than at that at pH 7.4, indicating that drug diffusion from scaffolds is related to the pH value of the medium. This may be because the amino groups of ChNCs in an acidic PBS solution are easily protonated. Electrostatic repulsion was caused by cationic amino groups ($-NH_3^+$) of adjacent ChNC molecules, which makes the scaffold swell, and a greater amount of curcumin can be released from a swollen scaffold. Hence, the drug diffuses more easily from scaffolds at a lower pH.[52] All results suggest that XChNC scaffolds with high porosity and nanostructure are beneficial to drug loading and sustained release.

Cytotoxicity of Curcumin-XChNC Scaffolds. MCF-7 cells were used as model cells to evaluate the effect of curcumin released from scaffolds in vitro because curcumin is an anticancer drug. Figure 9 shows images of MCF-7 cells stained with AO/EB reagent after cells were cultured on XChNC and curcumin-XChNC scaffolds for 24 and 72 h. MCF-7 cells exhibited good cell conditions, with no dead cells observed in the control group after 24 h, and MCF-7 cells proliferated exponentially after being cultured for 72 h. MCF-7 cells grew well on XChNC scaffolds and clearly proliferated for 72 h, suggesting that there was no toxicity caused by the pure scaffold. In contrast, several orange cells were observed on curcumin-XChNC scaffolds at 24 h, indicating that curcumin released from scaffolds induced apoptosis of the cancer cells. Furthermore, it can also be observed that there were fewer proliferated MCF-7 cells on curcumin-XChNC scaffolds at 72 h than those on XChNC scaffolds, and almost all MCF-7 cells were stained orange. These results indicate that released curcumin can inhibit the growth of MCF-7 cells and has a sustainable killing effect on cancer cells.

CCK-8 assay was used to evaluate the cell viability of MCF-7 cells cultured on XChNC and curcumin-XChNC scaffolds. As

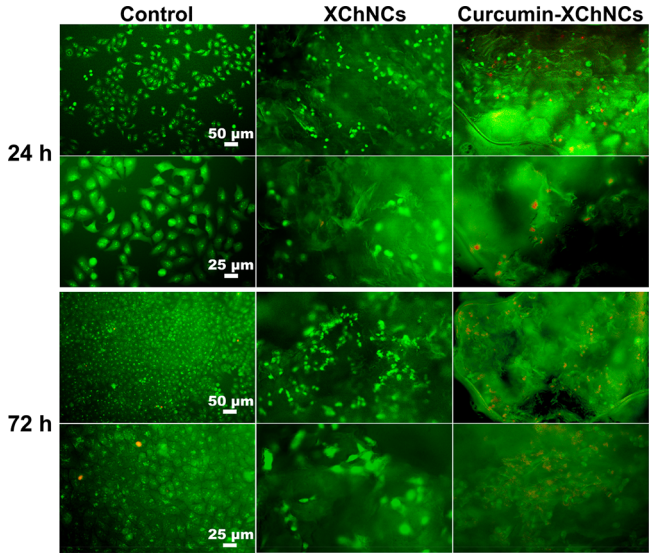

Figure 9. Fluorescence images of MCF-7 cells on XChNC and curcumin-XChNC scaffolds.

shown in Figure 10, the cell viabilities on XChNC scaffolds at 1, 3, and 5 days were 79.8, 80.7, and 81.2%, respectively,

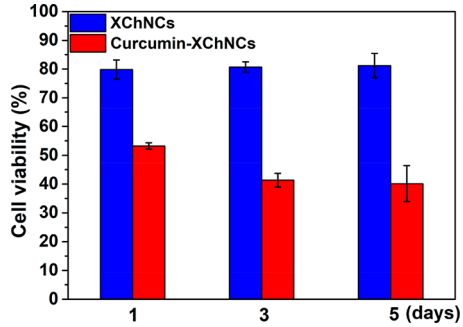

Figure 10. Cell viability of MCF-7 cells incubated with XChNC and curcumin-XChNC scaffolds for 1, 3, and 5 days.

indicating that there was no anticancer activity observed with XChNCs. In contrast, the cell viabilities on curcumin-XChNC scaffolds at 1, 3, and 5 days were 53.2, 41.3, and 40.1%, respectively. Compared to XChNC scaffolds, the cell viability of drug-loaded XChNC scaffolds was much lower. The cell viability significantly decreased after 5 days of culture due to

DOI: 10.1021/acsanm.8b01585
ACS Appl. Nano Mater. 2018, 1, 6790−6799

the effects of the drug. These CCK-8 results are consistent with the fluorescence images shown above. Overall, all of these results indicate that curcumin-XChNC scaffolds have good anticancer properties and are a potential material for anticancer drug-delivery carriers.

CONCLUSIONS

ChNCs with a rodlike morphology were successfully prepared from biodegradable crab shells and then used for the fabrication of porous ChNC scaffolds by freeze-drying. XChNC scaffolds were then obtained by cross-linking ChNCs with glutaraldehyde to enhance their stability in water. ChNC dispersions had good stability and colloidal behavior, which improved the physicochemical properties of porous XChNC scaffolds. The XChNC scaffold exhibited excellent properties, such as high mechanical strength, ultralight density, high porosity, and a tunable water absorption rate. The release study indicated a burst release of curcumin from scaffolds in the first 60 min, and sustained release was achieved in PBS until 600 min (pH 5.3 and 7.4). In vitro cytotoxicity assays showed that released curcumin could sustainably inhibit the proliferation of MCF-7 cells. All of the results suggest that porous XChNC scaffolds are promising materials for tissue-engineering and drug-delivery applications.

ASSOCIATED CONTENT

Supporting Information

The Supporting Information is available free of charge on the ACS Publications website at DOI: 10.1021/acsanm.8b01585.

Storage modulus, loss modulus, and dynamic viscosity of different concentrations of ChNC dispersions, photographs of ChNC and XChNC scaffolds immersed in serum solution and PBS, and a summary of the mechanical properties of XChNC scaffolds (PDF)

AUTHOR INFORMATION

Corresponding Author

*E-mail: liumx@jnu.edu.cn (M.L.).

ORCID

Mingxian Liu: 0000-0002-5466-3024

Notes

The authors declare no competing financial interest.

ACKNOWLEDGMENTS

This work was financially supported by the National Natural Science Foundation of China (Grants 51473069 and 51502113), the National High Technology Research and Development Program of China (Grant 2015AA020915), the Guangdong Special Support Program (Grant 2014TQ01C127), the Science and Technology Planning Project of Guangdong Province (Grant 2014A020217006), the Pearl River S&T Nova Program of Guangzhou (Grant 201610010026), and Guangdong Province Ocean and Fisheries Bureau-Key Technology Research and Development Program (Grant A201701A02).

REFERENCES

(1) Zeng, J. B.; He, Y. S.; Li, S. L.; Wang, Y. Z. Chitin Whiskers: An Overview. *Biomacromolecules* **2012**, *13*, 1−11.

(2) Chen, P.-Y.; Lin, A. Y.-M.; McKittrick, J.; Meyers, M. A. Structure and Mechanical Properties of Crab Exoskeletons. *Acta Biomater.* **2008**, *4*, 587−596.

(3) Raabe, D.; Sachs, C.; Romano, P. The Crustacean Exoskeleton as an Example of a Structurally and Mechanically Graded Biological Nanocomposite Material. *Acta Mater.* **2005**, *53*, 4281−4292.

(4) Merzendorfer, H.; Zimoch, L. Chitin Metabolism in Insects: Structure, Function and Regulation of Chitin Synthases and Chitinases. *J. Exp. Biol.* **2003**, *206*, 4393−4412.

(5) Pakzad, A.; Parikh, N.; Heiden, P. A.; Yassar, R. S. Revealing the 3D Internal Structure of Natural Polymer Microcomposites Using X-Ray Ultra Microtomography. *J. Microsc.* **2011**, *243*, 77−85.

(6) Salaberria, A. M.; Labidi, J.; Fernandes, S. C. M. Chitin Nanocrystals and Nanofibers as Nano-Sized Fillers into Thermoplastic Starch-Based Biocomposites Processed by Melt-Mixing. *Chem. Eng. J.* **2014**, *256*, 356−364.

(7) Fan, Y.; Saito, T.; Isogai, A. Chitin Nanocrystals Prepared by Tempo-Mediated Oxidation of Alpha-Chitin. *Biomacromolecules* **2008**, *9*, 192−198.

(8) Fan, Y.; Saito, T.; Isogai, A. Preparation of Chitin Nanofibers from Squid Pen Beta-Chitin by Simple Mechanical Treatment under Acid Conditions. *Biomacromolecules* **2008**, *9*, 1919−1923.

(9) Liu, M.; Zheng, H.; Chen, J.; Li, S.; Huang, J.; Zhou, C. Chitosan-Chitin Nanocrystals Composite Scaffolds for Tissue Engineering. *Carbohydr. Polym.* **2016**, *152*, 832−840.

(10) Gopalan Nair, K.; Dufresne, A. Crab Shell Chitin Whisker Reinforced Natural Rubber Nanocomposites. 2. Mechanical Behavior. *Biomacromolecules* **2003**, *4*, 666−674.

(11) Junkasem, J.; Rujiravanit, R.; Grady, B. P.; Supaphol, P. X-Ray Diffraction and Dynamic Mechanical Analyses of α-Chitin Whisker-Reinforced Poly(Vinyl Alcohol) Nanocomposite Nanofibers. *Polym. Int.* **2010**, *59*, 85−91.

(12) Liu, Y.; Wu, F.; Zhao, X.; Liu, M. High-Performance Strain Sensors Based on Spirally Structured Composites with Carbon Black, Chitin Nanocrystals, and Natural Rubber. *ACS Sustainable Chem. Eng.* **2018**, *6*, 10595−10605.

(13) Zhou, J.; Butchosa, N.; Jayawardena, H. S.; Zhou, Q.; Yan, M.; Ramström, O. Glycan-Functionalized Fluorescent Chitin Nanocrystals for Biorecognition Applications. *Bioconjugate Chem.* **2014**, *25*, 640−643.

(14) Tzoumaki, M. V.; Moschakis, T.; Kiosseoglou, V.; Biliaderis, C. G. Oil-in-Water Emulsions Stabilized by Chitin Nanocrystal Particles. *Food Hydrocolloids* **2011**, *25*, 1521−1529.

(15) Li, H. Y.; Li, H.; Wang, B. J.; Gu, Q.; Jiang, Z. Q.; Wu, X. D. Synthesis and Properties of Poly(3-Hydroxybutyrate-Co-3-Hydroxyvalerate)/Chitin Nanocrystals Composite Scaffolds for Tissue Engineering. *Chin. Chem. Lett.* **2014**, *25*, 1635−1638.

(16) Gayathri, N. K.; Aparna, V.; Maya, S.; Biswas, R.; Jayakumar, R.; Mohan, C. G. Preparation, Characterization, Drug Release and Computational Modelling Studies of Antibiotics Loaded Amorphous Chitin Nanoparticles. *Carbohydr. Polym.* **2017**, *177*, 67−76.

(17) Zhao, Y.; Chen, G.; Sun, M.; Jin, Z.; Gao, C. Study on Preparation of the pH Sensitive Hydroxyethyl Chitin/Poly (Acrylic Acid) Hydrogel and its Drug Release Property. *J. Biomed. Eng.* **2006**, *23*, 338−341.

(18) Evdokimova, O. L.; Svensson, F. G.; Agafonov, A. V.; Håkansson, S.; Seisenbaeva, G. A.; Kessler, V. G. Hybrid Drug Delivery Patches Based on Spherical Cellulose Nanocrystals and Colloid Titania-Synthesis and Antibacterial Properties. *Nanomaterials* **2018**, *8*, 228.

(19) Wang, H.; He, J.; Zhang, M.; Tam, K. C.; Ni, P. A New Pathway Towards Polymer Modified Cellulose Nanocrystals via a "Grafting onto" Process for Drug Delivery. *Polym. Chem.* **2015**, *6*, 4206−4209.

(20) Ndong Ntoutoume, G. M. A.; Granet, R.; Mbakidi, J. P.; Brégier, F.; Léger, D. Y.; Fidanzi-Dugas, C.; Lequart, V.; Joly, N.; Liagre, B.; Chaleix, V.; Sol, V. Development of Curcumin-Cyclodextrin/Cellulose Nanocrystals Complexes: New Anticancer Drug Delivery Systems. *Bioorg. Med. Chem. Lett.* **2016**, *26*, 941−945.

(21) Wang, H.; Roman, M. Formation and Properties of Chitosan-Cellulose Nanocrystal Polyelectrolyte-Macroion Complexes for Drug Delivery Applications. *Biomacromolecules* **2011**, *12*, 1585−1593.

DOI: 10.1021/acsanm.8b01585
ACS Appl. Nano Mater. 2018, 1, 6790−6799

(22) Tong, W. Y.; bin Abdullah, A. Y. K.; binti Rozman, N. A. S.; bin Wahid, M. I. A.; Hossain, M. S.; Ring, L. C.; Lazim, Y.; Tan, W. N. Antimicrobial Wound Dressing Film Utilizing Cellulose Nanocrystal as Drug Delivery System for Curcumin. *Cellulose* **2018**, *25*, 631−638.
(23) Abo-Elseoud, W. S.; Hassan, M. L.; Sabaa, M. W.; Basha, M.; Hassan, E. A.; Fadel, S. M. Chitosan Nanoparticles/Cellulose Nanocrystals Nanocomposites as a Carrier System for the Controlled Release of Repaglinide. *Int. J. Biol. Macromol.* **2018**, *111*, 604−613.
(24) Pande, V.; Kharde, A.; Bhawar, P.; Abhale, V. Scaffolds: Porous Scaffold for Modulated Drug Delivery. *Austin. Ther.* **2016**, *3*, 1027.
(25) Garg, T.; Rath, G.; Goyal, A. K. Biomaterials-Based Nanofiber Scaffold: Targeted and Controlled Carrier for Cell and Drug Delivery. *J. Drug Target.* **2015**, *23*, 202−221.
(26) Li, W.; Lan, Y.; Guo, R.; Zhang, Y.; Xue, W.; Zhang, Y. In Vitro and in Vivo Evaluation of a Novel Collagen/Cellulose Nanocrystals Scaffold for Achieving the Sustained Release of Basic Fibroblast Growth Factor. *J. Biomater. Appl.* **2015**, *29*, 882−893.
(27) Guo, R.; Lan, Y.; Xue, W.; Cheng, B.; Zhang, Y.; Wang, C.; Ramakrishna, S. Collagen-Cellulose Nanocrystal Scaffolds Containing Curcumin-Loaded Microspheres on Infected Full-Thickness Burns Repair. *J. Tissue Eng. Regener. Med.* **2017**, *11*, 3544−3555.
(28) Nguyen, V. C.; Nguyen, V. B.; Hsieh, M. F. Curcumin-Loaded Chitosan/Gelatin Composite Sponge for Wound Healing Application. *Int. J. Polym. Sci.* **2013**, *2013*, 106570.
(29) Dai, M.; Zheng, X.; Xu, X.; Kong, X.; Li, X.; Guo, G.; Luo, F.; Zhao, X.; Wei, Y. Q.; Qian, Z. Chitosan-Alginate Sponge: Preparation and Application in Curcumin Delivery for Dermal Wound Healing in Rat. *J. Biomed. Biotechnol.* **2009**, *2009*, 595126.
(30) Naseri, N.; Algan, C.; Jacobs, V.; John, M.; Oksman, K.; Mathew, A. P. Electrospun Chitosan-Based Nanocomposite Mats Reinforced with Chitin Nanocrystals for Wound Dressing. *Carbohydr. Polym.* **2014**, *109*, 7−15.
(31) Wongpanit, P.; Sanchavanakit, N.; Pavasant, P.; Bunaprasert, T.; Tabata, Y.; Rujiravanit, R. Preparation and Characterization of Chitin Whisker-Reinforced Silk Fibroin Nanocomposite Sponges. *Eur. Polym. J.* **2007**, *43*, 4123−4135.
(32) Mathew, A. P.; Laborie, M. P.; Oksman, K. Cross-Linked Chitosan/Chitin Crystal Nanocomposites with Improved Permeation Selectivity and pH Stability. *Biomacromolecules* **2009**, *10*, 1627−1632.
(33) Yang, Y.; Ritchie, A. C.; Everitt, N. M. Comparison of Glutaraldehyde and Procyanidin Cross-Linked Scaffolds for Soft Tissue Engineering. *Mater. Sci. Eng., C* **2017**, *80*, 263−273.
(34) Ratanajiajaroen, P.; Watthanaphanit, A.; Tamura, H.; Tokura, S.; Rujiravanit, R. Release Characteristic and Stability of Curcumin Incorporated in β-Chitin Non-Woven Fibrous Sheet Using Tween 20 as an Emulsifier. *Eur. Polym. J.* **2012**, *48*, 512−523.
(35) Ma, Q.; Cao, L.; Liang, T.; Li, J.; Lucia, L. A.; Wang, L. Active Tara Gum/PVA Blend Films with Curcumin-Loaded CTAC Brush-Tempo-Oxidized Cellulose Nanocrystals. *ACS Sustainable Chem. Eng.* **2018**, *6*, 8926−8934.
(36) Revol, J. F.; Marchessault, R. H. In Vitro Chiral Nematic Ordering of Chitin Crystallites. *Int. J. Biol. Macromol.* **1993**, *15*, 329−335.
(37) Huang, Y.; Yao, M.; Zheng, X.; Liang, X.; Su, X.; Zhang, Y.; Lu, A.; Zhang, L. Effects of Chitin Whiskers on Physical Properties and Osteoblast Culture of Alginate Based Nanocomposite Hydrogels. *Biomacromolecules* **2015**, *16*, 3499−3507.
(38) Yamamoto, Y.; Nishimura, T.; Saito, T.; Kato, T. $CaCO_3$/Chitin-Whisker Hybrids: Formation of $CaCO_3$ Crystals in Chitin-Based Liquid-Crystalline Suspension. *Polym. J.* **2010**, *42*, 583−586.
(39) Nge, T. T.; Hori, N.; Takemura, A.; Ono, H.; Kimura, T. Phase Behavior of Liquid Crystalline Chitin/Acrylic Acid Liquid Mixture. *Langmuir* **2003**, *19*, 1390−1395.
(40) Liu, D.; Wang, S.; Ma, Z.; Tian, D.; Gu, M.; Lin, F. Structure-Color Mechanism of Iridescent Cellulose Nanocrystal Films. *RSC Adv.* **2014**, *4*, 39322−39331.
(41) Liu, D.; Chang, Y.; Tian, D.; Wu, W.; Lu, A.; Prempeh, N.; Tan, M.; Huang, Y. Lyotropic Liquid Crystal Self-Assembly of H_2O_2-Hydrolyzed Chitin Nanocrystals. *Carbohydr. Polym.* **2018**, *196*, 66−72.
(42) Liu, Y.; Liu, M.; Yang, S.; Luo, B.; Zhou, C. Liquid Crystalline Behaviors of Chitin Nanocrystals and Their Reinforcing Effect on Natural Rubber. *ACS Sustainable Chem. Eng.* **2018**, *6*, 325−336.
(43) Yan, W. X.; Sheng, L. B.; Ya-Li, J. I. Preparation and Rheological Behavior of Chitin Nanowhisker/Chitosan Blend Solution. *J. Donghua Univ.* **2015**, *41*, 277−281.
(44) Lin, N.; Zhao, S.; Gan, L.; Chang, P. R.; Xia, T.; Huang, J. Preparation of Fungus-Derived Chitin Nanocrystals and their Dispersion Stability Evaluation in Aqueous Media. *Carbohydr. Polym.* **2017**, *173*, 610−618.
(45) Li, Y.; Liu, T.; Zheng, J.; Xu, X. Glutaraldehyde-Crosslinked Chitosan/Hydroxyapatite Bone Repair Scaffold and its Application as Drug Carrier for Icariin. *J. Appl. Polym. Sci.* **2013**, *130*, 1539−1547.
(46) Yuan, N.-Y.; Lin, Y.-A.; Ho, M.-H.; Wang, D.-M.; Lai, J.-Y.; Hsieh, H.-J. Effects of the Cooling Mode on the Structure and Strength of Porous Scaffolds Made of Chitosan, Alginate, and Carboxymethyl Cellulose by the Freeze-Gelation Method. *Carbohydr. Polym.* **2009**, *78*, 349−356.
(47) Huang, Y.; Yang, J.; Chen, L.; Zhang, L. Chitin Nanofibrils to Stabilize Long-Life Pickering Foams and their Application for Lightweight Porous Materials. *ACS Sustainable Chem. Eng.* **2018**, *6*, 10552−10561.
(48) Ifuku, S.; Nogi, M.; Abe, K.; Yoshioka, M.; Morimoto, M.; Saimoto, H.; Yano, H. Preparation of Chitin Nanofibers with a Uniform Width as α-Chitin from Crab Shells. *Biomacromolecules* **2009**, *10*, 1584−1588.
(49) Monteiro, O. A. C.; Airoldi, C. Some Studies of Crosslinking Chitosan-Glutaraldehyde Interaction in a Homogeneous System. *Int. J. Biol. Macromol.* **1999**, *26*, 119−128.
(50) Yallapu, M. M.; Jaggi, M.; Chauhan, S. C. β-Cyclodextrin-Curcumin Self-Assembly Enhances Curcumin Delivery in Prostate Cancer Cells. *Colloids Surf., B* **2010**, *79*, 113−125.
(51) Anitha, A.; Maya, S.; Deepa, N.; Chennazhi, K. P.; Nair, S. V.; Tamura, H.; Jayakumar, R. Efficient Water Soluble-Carboxymethyl Chitosan Nanocarrier for the Delivery of Curcumin to Cancer Cells. *Carbohydr. Polym.* **2011**, *83*, 452−461.
(52) Prabaharan, M.; Reis, R. L.; Mano, J. F. Carboxymethyl Chitosan-Graft -Phosphatidylethanolamine: Amphiphilic Matrices for Controlled Drug Delivery. *React. Funct. Polym.* **2007**, *67*, 43−52.

DOI: 10.1021/acsanm.8b01585
ACS Appl. Nano Mater. 2018, 1, 6790−6799